HHS Public Access

Author manuscript

Arch Biochem Biophys. Author manuscript; available in PMC 2018 January 01.

Published in final edited form as:

Arch Biochem Biophys. 2017 January 01; 613: 1–11. doi:10.1016/j.abb.2016.10.017.

Probing the orientation of inhibitor and epoxy-eicosatrienoic acid binding in the active site of soluble epoxide hydrolase

Kin Sing Stephen Lee[a], **Niel M. Henriksen**[b], **Connie J. Ng**[a], **Jun Yang**[a], **Weitao Jia**[c], **Christophe Morisseau**[a], **Armann Andaya**[c], **Michael K. Gilson**[b], and **Bruce D. Hammock**[a]

[a] Department of Entomology and Nematology, UCD Comprehensive Cancer Center, University of California at Davis, One Shields Avenue, Davis, California, CA 95616, U.S.A.

[b] Skaggs School of Pharmacy and Pharmaceutical Sciences, University of California at San Diego, 9500 Gilman Drive, MC 0736, La Jolla, CA 92093, U.S.A.

[c] Campus Mass Spectrometry Facilities, University of California at Davis, One Shields Avenue, Davis CA 95616, U.S.A.

Abstract

Soluble epoxide hydrolase (sEH) is an important therapeutic target of many diseases, such as chronic obstructive pulmonary disease (COPD) and diabetic neuropathic pain. It acts by hydrolyzing and thus regulating specific bioactive long chain polyunsaturated fatty acid epoxides (lcPUFA), like epoxyeicosatrienoic acids (EETs). To better predict which epoxides could be hydrolyzed by sEH, one needs to dissect the important factors and structural requirements that govern the binding of the substrates to sEH. This knowledge allows further exploration of the physiological role played by sEH. Unfortunately, a crystal structure of sEH with a substrate bound has not yet been reported. In this report, new photoaffinity mimics of a sEH inhibitor and EET were prepared and used in combination with peptide sequencing and computational modeling, to identify the binding orientation of different regioisomers and enantiomers of EETs into the catalytic cavity of sEH. Results indicate that the stereochemistry of the epoxide plays a crucial role in dictating the binding orientation of the substrate.

Graphical abstract

Corresponding Author: Bruce D. Hammock, Department of Entomology and Nematology, UCD Comprehensive Cancer Center, University of California at Davis, One Shields Avenue, Davis, CA 95616. Tel: 530 752-7519, Fax: 530-752-1537, bdhammock@ucdavis.edu.

Disclosure Statement

Bruce D. Hammock is the founder of Eicosis L.C.C. The goal of Eicosis L.C.C. is to advance sEH inhibitor to the clinic.

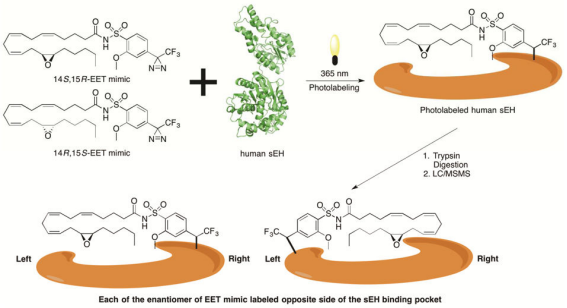

Keywords

photoaffinity tag; photolabel; soluble epoxide hydrolase; epoxyeicosatrienoic acid; computational simulation; peptide sequencing

Introduction

Soluble epoxide hydrolase (sEH, EC 3.3.2.10) degrades saturated and long-chain polyunsaturated fatty acid (lcPUFAs) epoxides to the corresponding 1,2-diols.[1] The lcPUFA epoxides from both omega-3 and omega-6 lcPUFAs play an important role in human physiology and health. Studies have shown that lcPUFA epoxides are anti-inflammatory, anti-hypertensive, organ protective and analgesic.[2-9] Therefore, stabilization of lcPUFA epoxides *in vivo* through sEH inhibition is generally beneficial to human health and certain diseases, like chronic obstructive pulmonary diseases (COPD),[10, 11] atrial fibrillation[12] and diabetic neuropathic pain.[13-15]. To better predict whether an epoxide could be hydrolyzed by sEH, one needs to dissect the structural requirements that dictate the binding of substrate into the sEH active site. This will help us to identify other potential substrates for sEH including both endogenous and xenobiotic epoxides, which could affect its known biological roles as well as explore new roles played by sEH in human health and xenobiotic metabolism.

Over the years, numerous crystal structures of the sEH with various structurally different inhibitors have been solved. [13, 16-21] Although these *holo*-structures helped us to design better inhibitors, [13] these structures provide little information on how substrates bind to sEH, particularly lcPUFA epoxides. In addition, the substrate bound sEH structure has not yet been solved. To make matters more complicated, several crystal structures show that inhibitors with very similar structure bind to sEH with opposite orientations (**Figure S1**). [22] These data suggest that the sEH inhibitors and substrates may bind to sEH with multiple orientations so that a crystal structure may not be able to capture all the orientations. These data also illustrate a limitation of crystallography and the need for new complementary approaches to elucidate mechanistic details of the binding of substrates and inhibitors to sEH. Therefore, in this study, computational models in combination with photoaffinity labeling experiments were conducted in order to better understand how EET bind to the active site of sEH.

Over the years, computational approach has been used successfully to study the molecular details that govern the binding of substrates in the active site of the enzymes. It has also been used to identify new structural scaffold for drug design. [23-31] Molecular docking or molecular dynamics simulation have been used to identify potent inhibitors for sEH. [28, 32-34] Moreover, the catalytic mechanism of sEH on model substrates was well studied by computational models.[35-38] Therefore, computational model provides a complementary approach for us to investigate the molecular details on how EET binds to the active site of sEH.

Besides, photoaffinity labels in combination with proteomics or radiotracers have become important tools to identify specific binding proteins of the ligand or to locate specific interactions or the orientation of the ligand in the target protein. [39-42] In this report, photolabel mimics of sEH inhibitors (mimic **7**) and two endogenous substrates, epoxy-eicosatrienoic acids (EETs) were prepared (mimic **16** and mimic **17**) (Figure **1**). These mimics, in combination with peptide sequencing and computational modeling, were used 1) to test whether the inhibitor in general has several binding orientations in the sEH binding pocket, 2) to identify the binding orientation of different regioisomers of EETs in sEH binding pocket, 3) to test if carboxylate or other structural features play an important role in binding to sEH and 4) to test the hypothesis that the binding of the potent transition state mimic to sEH results a different arrangement of active site residues as compared to the binding of the substrate to sEH. In addition, the stable photolabel mimic of a tight binding sEH inhibitor allows us to optimize the conditions for photolabeling sEH with the photolabel of the substrate.

Materials and Methods

Experimental procedures for the syntheses of the compounds used in this manuscript are described in detail in supporting information.

A. Experimental for Biochemistry

1. Enzyme Preparation

Human recombinant sEH: The purification and expression of human soluble epoxide hydrolase (sEH) was described previously followed a published procedure. [43] Briefly, the human sEH was expressed in a baculovirus system in high yield. The human sEH in cell lysate was then purified by affinity chromatography and yielded a fraction with high specific activity and apparent homogeneity on SDS-PAGE (>95%) (**Figure S16**). The enzyme was then quickly frozen in liquid nitrogen and stored at −78°C. The enzyme was thawed slowly on ice before use.

***Bacterial* cytochrome *P450 (BM3-F87V)*:** In order to synthesized the regio- and stereo-specific 14*S*,15*R*-EET, a bacterial cytochrome P450 mutant (BM3-F87V) was used. The expression and purification of BM3-F87V was based on a published procedure. [44] Briefly, the plasmid containing bacterial P450 BM3-F87V was a generous gift from Prof. Frances A. Walker at the University of Arizona and was transformed to *E. coli* strain DH5α competent cells (Invitrogen™) according to the manufacture's protocol. The transformed cells were

used for protein expression. A single colony of DH5α containing the plasmid of BM3-F87V was inoculated into 5mL of LB/Ampiclin (100μg/mL). The cell culture was incubated at 37°C and shaken at 220 rpm for 12h. The cell culture (5 mL) was then inoculated into 1.5L of LB/Ampicilin (100 μg/mL). The larger cell culture was then incubated at 37°C and shaken at 220 rpm for 8h until the OD_{600} reached around 0.8 to 1.0. The cell culture was then further incubated at 30°C and shaken at 220 rpm for an additional 16h.

Cells were harvested at 4°C by centrifugation for 30 min at 7000 rpm. The supernatant was discarded and the lysate buffer (100 mM Tris-HCl, 1 mM 1,14-dithiothreitol, 0.1 mM ethylenediaminetetraacetic acid, 0.1 mM PMSF, 40 mL) was added and the cells were resuspended in the lysate buffer at 4°C. The cells were then frozen at −78°C for 24h. The cells were warmed up slowly in an ice bath. Once the cells were thawed, the cells were lyzed by sonication (Fisher Scientific Sonic Dismembrator Model 100, power 10, 60s on followed by 60s off for 5 times). The cell lysate was then centrifuged at 20,000g for 30 min at 4°C and the supernatant was transferred to another clean centrifuge tube and further centrifuged at 20,000g for 30 min at 4°C. The supernatant was then loaded into a column (2.5 × 20 cm) packed with anion-exchange resin (GE Healthcare Life Sciences, Q Sepharose Fast Flow). The column was washed with 5 column volumes of wash buffer (100 mM Tris-HCl, pH 7.8) followed by 5 column volumes of elution buffer (100 mM Tris-HCl, 175 mM NaCl, pH 7.8) and ended with 10 column volumes of cleaning buffer (100 mM Tris-HCl, 340 mM NaCl, pH 7.8). The red fractions were collected. The fractions were combined and concentrated using a centrifuge filter (Amicon Ultra-15, cutoff <50 KDa). The concentrated enzyme solution was assayed according to the published procedure. [45] The purified enzyme was mixed with glycerol in equal volume and frozen with liquid nitrogen. The enzyme was stored at −78°C until used.

2. IC_{50} measurement for inhibitor mimic on human sEH—The IC_{50}s of the inhibitor mimic **7** and UC2389 were determined by a radiometric assay using a tritium labeled substrate named [2-^{3}H]-*trans*-1,3-diphenylpropene oxide (*t*DPPO) according to the published procedure. [46] The experiment was done in an environment with ambient light setting to prevent the activation of the photoaffinity label. Briefly, human sEH (2.5 nM, 100 mM sodium phosphate, pH = 7.4, 0.1 mg/mL bovine serum albumin) was pre-incubated at 30 °C for 5 min with the mimic **7** at different concentration (0.7 nM to 1 uM). At time = 0, *t*DPPO (1 μL, 5 mM in DMSO, 10,000 cpm/μL) was added and the reaction mixture was shaken in an incubator (100 rpm, 30 °C) for 10 min. The reaction was quenched by an addition of methanol (60 μL) and *iso*-octane (200 μL). The mixture was vortexed vigorously for 1 min for three times to ensure fully mixing. The mixture was then centrifuged (4000 rpm, 5 min, rt). The aqueous layer (40 μL) was withdrawn and transferred to a scintillation solution (Fisher Chemical, ScintiVerse ™ BD Cocktail, 1mL). The mixture was mixed vigorously for 1 min and the radioactivity was measured with a liquid scintillation counter (PerkinElmer Tri-Carb 2810 TF Liquid Scintillation Analyzer). The IC_{50}s were determined based on regression of at least five datum points with at least two points on either side of the IC_{50}s in the linear region of the curve. The results were the average of duplicated measurements.

3. Photoaffinity labeling experiments

Rate of photolysis of mimic 7: Mimic **7** solution (100 μM, methanol, 2 mL) in a 10 mL test tube, was incubated on ice for 20 min in dim red light. The solution on ice bath was placed 5 cm above the transilluminator (AlphaImager System, 365/302 nm UV transilluminator) and was irradiated at 365 nm. After each of the 1 min irradiation, the solution was incubated on ice in the dark for 2 min before the next irradiation. The UV-vis spectra (200 to 600 nm) were recorded at irradiation time = 0, 1 and 3 min.

The stability test of mimic 7 under ambient light: Mimic **7** solution (100 μM, methanol, 2 mL) in a 10 mL test tube, was incubated on ice for 20 min in dim red light. The solution was then incubated on ice under the ambient light. The UV-vis spectra (200 to 600 nm) were recorded at time = 0, 10, 20 min and 5 h.

Optimization of the mimic 7 to hsEH ratio for photoaffinity labeling experiment: Mimic **7** at desired concentration (50, 25, 12.5, 5 μM) was incubated with human sEH (5 μM, 100 mM sodium phosphate, pH 7.4, 400 μL) at rt for 1.5h. The mixtures were then incubated on ice for 30 min before irradiation at 365 nm. The mixtures were then placed 5 cm above the transilluminator (AlphaImager System, 365/302 nm UV transilluminator) and were irradiated at 365 nm for 2 min. The samples were then concentrated with a centrifugal filter (Amicon Ultra, 0.5 mL, 10KDa) to approximately 30 μL. The samples were then quickly frozen with liquid nitrogen and were stored at −78 °C before mass spectrometry analysis.

Intact protein mass spectrometry analysis: The samples were injected into the electrospray mass spectrometry (Parameter listed in **Table E1**) through a desalting column (Phenomenex Jupiter® C4, 300Å, 50 × 4.6 mm, particle size: 5 μm) with the gradient condition stated in **Table E2**.

The rate of hydrolysis of mimic 16 and 17 by hsEH: Human sEH (200 nM, 100 mM sodium phosphase, pH 7.4, 1 mL) was incubated on ice for 10 min. Mimic **16** and **17** (20 mM, 1μL, EtOH) was added and the reaction mixture was vortexed. The samples (10 μL) were collected at time 0, 0.5, 1, 2, 5, 10, 20, 30, 40 and 60 min. The collected samples were immediately added to methanol (90 μL). The suspension was centrifuged (4000 rpm, 5 min, rt). The supernatant was transferred to the HPLC vials (Phenomenex, 1.5 mL) and the samples were stored at −20 °C before LC/MS-MS analysis. The results were an average of duplicated results.

The sample was injected into a triple quadrupole mass spectrometer (Parameter listed in **Table E4**) through a HPLC column (Phenomenex Kinetex Evo C18, 100Å, 50 × 2.1 mm, particle size: 2.6 μm) with the LC gradient condition stated in **Table E3**.

Photoaffinity labeling of human sEH with EET-PAL mimics: EET-PAL (25 μM) in sodium phosphate buffer (100 mM sodium phosphate, pH 7.4, 10 mL) was incubated at 0°C for 20 min. Human sEH (20 μM, 100 mM sodium phosphate, pH 7.4, 10 μL) was added to the EET-PAL solution. The reaction mixture was vortexed for 15 s and immediately

incubated in an ice bath. The sample was placed 5 cm above the transilluminator (AlphaImager System, 365/302 nm UV transilluminator) and irradiated at 365 nm for 2 min. The reaction mixture was then incubated on ice bath for an additional 1 min. An addition of EET-PAL (50 mM, 5 μL) was added in the reaction mixture and vortexed for 15s. The mixture was immediately incubated in an ice bath, placed 5 cm above the transilluminator (AlphaImager System, 365/302 nm UV transilluminator) and irradiated at 365 nm for an addition 2 min. The sample was then concentrated with a centrifugal filter (Amicon Ultra, 0.5 mL, 10KDa) to approximately 30 μL. The sample was then frozen quickly with liquid nitrogen and was stored at −78 °C before mass spectrometry analysis.

Trypsin digestion protocol: The experiment was conducted according to the UC Davis Protease Max Ingel digestion protocol published on the website: (https://docs.google.com/document/d/1GdzZBVKUOfLjdWGvlfJNTS7mZ0su7ZJyAOOBPhk3l8s/edit). Briefly, the photoaffinity labeled sample (12.5 μg) was incubated in NuPAGE® LDS sample buffer (Invitrogen, 20 μL) at 100 °C for 5 min. The sample was then purified on Novex® Bolt 4-12% Bis-Tris Plus gel (Invitrogen®, 15 wells). The gel was stained with InstantBlue (Expedeon) and de-stained according to the vendor protocol. The stained band (~62KDa) was isolated and further cut into small pieces (1 mm^3). The gel fragments were washed with ammonium bicarbonate solution (AMBIC, 50 mM, 2× 500 μL, pH 8) and were dried with acetonitrile (2× 500 μL). The gel pieces were then swelled with dithiothreitol solution (10 mM, 50 mM AMBIC, 500 μL) for 30 min at 56 °C. The supernatant was removed. The gel pieces were then dehydrated with acetonitrile (2× 500 μL). The dehydrated gel pieces were then incubated in iodoacetamide solution (55 mM, 50 mM AMBIC, 500 μL) at rt for 20 min in the dark. The supernatant was removed. The gel pieces were then washed with AMBIC (50 mM, 500 μL). The supernatant was removed. The gel pieces were then dehydrated with acetonitrile (2 × 500 μL). The dehydrated gel pieces were further dried under a vacuum. The dried gel pieces were then rehydrated with a digestion buffer (Promega Trypsin Gold Mass Spectrometry Grade, 100μg/mL, 50 mM AMBIC, pH 8.0, 50 μL). AMBIC (50 mM, 200 μL) was added. The sample was then incubated at 37 °C for 12h. The supernatant was then transferred to a clean Eppendorf tube. Acetonitrile solution (60% acetonitrile in water with 0.1% trifluoroacetic acid, 200 μL) was added to the gel pieces and the resulting mixtures were sonicated in a water bath for 10 min at rt. The samples were centrifuged (14,000 rpm, 10 min, rt) and the supernatant was collected and was combined with the collected supernatant. The combined supernatant was concentrated under a vacuum. The sample was ready to be analyzed by LC/MS-MS.

Mass spectrometry analysis of soluble expoxide hydrolase tryptic digest: Nano-RPLC tandem mass spectrometric analysis was performed on an LTQ-OrbitrapXL mass spectrometer (ThermoFisher Scientific, San Jose, CA) equipped with an ADVANCE nanospray ion source (Michrom Bioresources, Auburn, CA), a Surveyor MS pump (ThermoFisher), and a microautosampler (ThermoFisher). The lyophillized tryptic peptide mixture was resuspended in 2% acetonitrile with 0.5% TFA and separated on a 100-μm-ID IntegraFrit" column (New Objective, Woburn, MA) packed in house with reversed-phase Magic C_{18}AQ material (15 cm length, 5 μm particle size, 200-Å pore size, Michrom Bioresources). Then the sample was loaded for 10 min at 2% solvent B (0.1% (v/v) formic

acid in ACN) and 98% solvent A (0.1% (v/v) formic acid in water) at a flow rate of 500 nL/min. Peptides were resolved by the following gradient at flow rate of 500 nL/min: 2–10% solvent B in 10 min, 10–40% solvent B in 60 min, 40–70% solvent B in 5 min, 70-85% solvent B in 2 min, maintained at 85% solvent B for 5 min, and then reversed to 2% solvent B. The LTQ-OrbitrapXL instrument methods were comprised of one MS scan followed by data dependent MS/MS scans of the six most intense precursors. Full MS scan was performed by the Orbitrap with resolution r=30,000 at m/z 400 to identify precursors for tandem mass spectrometry, and data dependent tandem mass spectrometry was performed by collisionally induced dissociation (CID) with the LTQ.

Peptide Identification via MASCOT Database Search: MASCOT software (version 2.2.07, Matrix Science, London, U.K.) was used for database searching. MASCOT DTA format files were converted from the RAW data files acquired for each LC-MS run using Bioworks Browser software (version 3.3.1 SP1, ThermoFisher). The resulting Sequest (.DTA) files from each run were merged into one single .MGF (Mascot Generic Format) file via merge.pl (version 2007.3.9, Matrix Science, London, U.K.) and searched against the entry for human bifunctional epoxide hydrolase. Searches were performed with tryptic specificity allowing one missed cleavage and a tolerance on the mass measurement of 15 ppm in MS mode and 0.5 Da for MS^2 ions. Possible structure modifications allowed were protein N-terminal acetylation, carbamidomethylation of Cys; oxidation of Met and custom label of all twenty amino acids. All identified peptides have an individual MS^2 ion score equal or greater than 18, corresponding to a statistically significant (p value < 0.05) confident identification which was set as default by MASCOT algorithm.

Enantioselectivity hydrolysis of 14,15-EET by human sEH: To the solution of human sEH (4 nM, 1mL, 100 mM sodium phosphate buffer with 0.1 mg/mL bovine serum albumin, pH 7.4), (±) 14,15-EET (50 μM, 10 μL) was added. The reaction was incubated at 37 °C and shaken at 100 rpm. At time = 0.25, 15, 30, 60, 90, 120 and 180 min, mixture (100 μL) was collected and was added to quenching solution (100 μL, methanol) and mixed vigorously on vortex mixer. The samples were centrifuged at 5000 g for 5 min. The supernatant was transferred to HPLC vial and was stored in −20C before analysis. The analyses of the samples were performed as described in “Synthesis of (5*Z*,8*Z*,11*Z*)-13-((2*S*,3*R*)-3-pentyloxiran-2-yl)trideca-5,8,11-trienoic acid (14*S*, 15*R*-EET)” in Section A.17 in the supporting material.

B. Experimental for Simulation and Modeling

1. Docking protocol—All docking was carried out using Dock6.7. [47] Docking of EETs to the human sEH was carried out on three conformations of the protein: a high-resolution inhibitor-bound crystal structure (PDB:4JNC), and two conformations selected from MD simulations in which an EET molecule was bound. The PDB:4JNC structure was chosen because it has high-resolution (1.96 Å) and does not contain the phosphatase domain. Therefore the structure is smaller and more computationally tractable for the MD simulations.[48] In addition, the conformation of the hydrolase domain are very similar across all the crystal structures that we have evaluated (C-alpha RMSD less than 0.6 Å). Initially, the protonation state of the histidine residues was determined by the H++ server,

[49] but we noticed an obvious clash between the protons on His239 and His251. These results led us to reevaluate protonation state of all the histidines in the structure. Taking into account of crystallographic waters, we assigned the following protonation states: 1) single protonation on the epsilon nitrogen for His239, His334, His420, His506 and His513; 2) single protonation on the delta nitrogen for His265 and, 3) double protonaton for His251, His518, and His524. In the end, only His239 and His334 were modified relative to the initial H++ assignment.

The preparation of the protein models for docking followed a standard Dock 6.7 approach. Briefly, the molecular surface was defined using a probe radius of 1.4 Å with the *DMS* program in UCSF Chimera.[50] The surface was populated with spheres, representing possible binding sites, using the Dock 6.7 accessory program *sphgen*.[51] Spheres beyond 12.0 Å of the input structure ligand were removed with the *sphere_selector* accessory program. A box enclosing the selected spheres by at least 12.0 Å was constructed with the *showbox* accessory program. Finally, a pre-computed interaction energy grid within the box was calculated with the *GRID* accessory program [52] using a 0.2 Å grid spacing, a bump overlap value of 0.75, and with the 6th- and 9th-exponential attractive and repulsion exponents, respectively. Charges and atom types of the ligand were assigned by AMBER's Antechamber program using the AM1-BCC charge method and SYBYL atom types.

For docking, most of the default Dock 6.7 settings were used with the exception of the following changes in order to make the pose searching more aggressive. Although it is more computationally expensive, manual matching instead of automated matching was used with a distance tolerance and minimum of 0.10 and 0.50, respectively. In addition, the maximum number of orientations was increased to 5000, the maximum number of anchors was reduced to 3 and, the maximum anchor size was reduced to 3 atoms. Because EET regioisomers do not have large rigid functional groups, the pruning settings were loosened to 2000 maximum orientations with a clustering cutoff value of 200 and score cutoff value of 200 kcal/mol. The translational and torsional step sizes were reduced to 0.5 Å and 5 degrees and 20 steps of torsional preminimization were added. Moreover, the maximum number of scored conformers was increased to 5000 and the cluster threshold value was decreased to 0.5 Å. A complete list of Dock 6.7 settings is provided in **Table S1**.

To ensure that the docking model was appropriate, we performed self-docking with the inhibitor in the PDB:4JNC structure and achieved a reasonable result. The top scoring pose had a RMSD to the crystal ligand of 1.3 Å (non-fluorine heavy atoms only), with the primary differences arising from a methylamine flip and an incorrect orientation of the amide group near the catalytic residues. The docking score is known to be rather qualitative and the docking was primarily used as a conformational search method in the present study. Therefore, it is perhaps more important to ensure that the docking poses with the correct orientation of the amide group scored in the top 9% and the docking poses with an RMSD of 0.4 Å relative to the crystallographic pose scored in the top 15%.

2. Molecular Dynamics Simulations—All molecular dynamics simulations were performed with the AMBER14 suite of programs. [53] The protein structure (PDB code: 4JNC) was used as the starting structure with the same histidine protonation states as

indicated in the Docking section. The system was parameterized with AMBER's ff14SB force field for the protein, GAFF 1.7 with AM1-BCC charges for the ligands, [54-56] TIP3P water, [57] and Joung/Cheatham parameters for net-neutralizing Na^+ and Cl^- ions. [58] Following parameterization of each ligand with GAFF, which is a force field designed to simulate small molecules, we performed an energy minimization of all ligands and compared the resulting structures with the semi-empirical AM1-BCC minimized structures to ensure that both method generated similar results. Each system contained 9100 TIP3P water molecules arranged to fit truncated octahedron periodic boundaries, which ensured a minimum of 12.0 Å between the solvent and the nearest box edge. Hydrogen mass repartitioning of the system PRMTOP file was accomplished with AMBER's Parmed program. This approach redistributes mass from heavy atoms to hydrogen atoms, leading to a reduction in the frequency of vibrations. This allows a longer time step without detectable changes in the thermodynamics[59, 60] and enables a 500 ns production simulation for each system with a 4 fs timestep. An 8 Å cutoff was used with default PME settings. Temperature control was maintained with the Langevin thermostat and constant pressure was enabled via the Monte-Carlo barostat.

The initial placement of the inhibitor was obtained via RMSD fit of the analogous crystal structure to the PDB:4JNC structure, when available (see **Table S2**). For inhibitors without a bound crystal structure and EET regioisomers, the initial bound conformation was generated by manually placing the ligand in the active site of sEH using a molecular visualization program (UCSF Chimera).[50] In this approach, the ligand was first overlaid on the bound ligand in PDB:4JNC structure using RMSD fit. Only the atoms in the functional group expected to bind to the hydrolase active site (i.e., urea, amide, amine, epoxide) were fitted. Following this step, any remaining steric clashes were resolved via manual rotation of the bonds in the tested ligands. After running production simulations, a semi-quantitative estimation of the binding free energy was made with MMGBSA analysis using the single trajectory approach. [61] The full production trajectory was sampled every 400 ps for MMGBSA analysis. Single-trajectory MMGBSA is an approximate endpoint free energy approach because it replaces any explicit solvent with an implicit solvent model and does not consider any of the solute entropy components. Thus, the values it produces are not expected to match the same magnitude of the experimental values, but can produce useful correlation, as seen in **Figure S9** in supporting information.

Result and Discussion

Design and Synthesis of sEH inhibitor Photoaffinity Mimic 7

In desinging the photolabel mimic used in this study, we sought to ensure that the mimic would bind to, the human sEH as well as the original ligand, UC2389, with minimization of non-specific labeling during the photolabeling experiment. Therefore, diazirine was selected as the photoactivated group because 1) unlike azide, it is activated at long wavelength UV (>355 nm) which minimizes the damage to the protein, 2) it is more stable than azide in the dark which prevents non-specific labeling, 3) it is small as compared to benzophenone which leads to less structural change to the mimic as compared to the original molecule and

4) the active specie of diazirine (carbene) has a much shorter half-life than either the activated azide or activated benzophenone which minimizes the non-specific labeling. [62]

Recently, a crystal structure of human sEH bound with a potent inhibitor (UC2389) which has a 1,3-disubstituted urea as central pharmacophore (**Figure 1**) was reported. [13] To test whether inhibitors with the general scaffold **X** (**Figure 1A**) bind to sEH in two different orientations, we designed and synthesized an mimic **7** of UC2389. In mimic **7**, the trifluoromethyl-group in **UC2389** was substituted by photolabel, trifluoromethyldiazirine, because of the structural similarity. (**Figure 1**) The synthesis of the 2389 mimic with photoaffinity tag is shown in **Scheme S1** in supporting information.

Optimization of the Experimental Conditions for the Photoaffinity Labeling human sEH

In order to test whether the replacement of trifluoromethyl-group with trifluoromethyldiazirine affects the binding of the mimic **7**, the IC_{50}s of mimic **7** (IC_{50} = 24.9±0.3 nM) and UC2389 (IC_{50} = 20.0±0.5 nM) were measured using a radiometric assay. [46] The potencies of **7** and UC2389 are very similar indicating that the replacement of trifluoromethyl- group with trifluoromethyldiazirine does not hinder the binding of the **7** to the sEH. We then optimized the photo-labeling reaction conditions. By monitoring the characteristic absorption peak of diazirine at 345 nm, the rate of photoactivation of the photolabel was measured. The results indicate that the mimic **7** (100 μM) is completely activated in less than 3 min by irradiation at 365 nm at 0 °C. (**Figure S3A**) Interestingly, the diazirine is very stable under ambient light at room temperature. (**Figure S3B**) The ratio of mimic **7** to sEH was then optimized for the photolabeling experiment. The results indicate that the optimum ratio between **7** and sEH is 10 to 1 because at this ratio, the majority of the sEH was mono-labeled although some doubly-labeled proteins were observed (around 10%). (**Figure 2A and Figure S5**) Finally, the reaction time was optimized, and as shown in **Figure 2B**, the majority of the human sEH is photolabeled by mimic **7** within the first 5 min, and the reaction does not proceed further after 10 min. Under the optimized conditions, our data showed that 75±0.5% of the sEH hydrolase activity was blocked irreversibly by **7** after photoactivation suggesting that at least 75% of the hydrolase domain of sEH was photolabeled by mimic **7**.

Only One Specific Peptide Fragment in Human sEH is Labeled by 7

The photolabeled sEH (**Figure 2C**) was subjected to trypsin digestion and further sequenced by LC/MS-MS. Based on the MASCOT analyses (minimum ion score 18 which equivalent to p = 0.05), only one singly labeled peptide (ion score = 70) was identified. (**Figure 2D and S10**) The results indicate that the labeled residues are located in close proximity to where the trifluoromethyl-group of UC2389 is positioned in the crystal structure (**Figure S4** and **S10**), [13] suggesting that inhibitors with general structure **X** (**Figure 1A**) are very likely to bind to human sEH in the same single orientation.

Design and Synthesis of the Photoaffinity Mimic of EET regioisomers

To understand the binding orientations of the endogenous substrates, like different regioisomers of EET, in the active site of human sEH, a similar strategy was pursued.

Therefore, mimics of different EET regioisomers carrying the photoaffinity label were designed and synthesized. (Figure **1**) In this study, we focused on 11,12-EET and 14,15-EET regioisomers because they are much better sEH substrates than 5,6-EET and 8,9-EET. [5]

The design principles of EET mimics include 1) the minimization of the overall structural modification, 2) bioisostere replacement of carboxylic acid of EET which allows the incorporation of the photoaffinity tag in the mimic and 3) the ease of the synthesis. Therefore, we would like to maintain the epoxide and the skipped polyene system in EETs. Falck *et al.* reported that the replacement of the carboxylic acid of the EETs with its bioisostere, acyl sulfonamide, is able to maintain the bioactivity of EETs in a vasodilation assay. [63] This is mainly due to the fact that pKa of the acidic proton of acyl sulfonamide (4.94) and the carboxylic acid (4.64) are very close. [64] This acidic proton appears to be the key for the activity of EET in a vasodilation assay [63] and herein we tested its importance on how EETs bind to sEH active site. In addition, the acyl sulfonamide provides a handle for us to attach a photoaffinity label in the mimic; thus, making it relatively easy to incorporate the trifluoromethyldiazirine into the EET mimics while maintaining the epoxide and the skipped polyene structure of the EETs. Therefore, EET mimics **16** and **17** were designed and synthesized and the syntheses of mimic **16** and **17** follow the general **Scheme S2** and **Scheme S3** in the supporting information.

11,12-EET-PAL 17 and 14,15-EET-PAL 16 Photolabeled the Peptide Fragments from Both Sides of the human sEH C-terminus Binding Pocket

As shown in **Figure 3A** and **S2**, 14,15-EET-PAL (**16**) and 11,12-EET-PAL (**17**) were quickly hydrolyzed by sEH to the corresponding 1,2-diol like 14,15-EET even at 4°C, suggesting that the addition of sulfonamide and photoaffinity label to the EET mimics does not interfere with the binding and the hydrolysis of the epoxide substrate. As predicted by the 10-fold different of kcat between 11,12-EET and 14,15-EET, 11,12-EET is hydrolyzed as much slower rate than 14,15-EET at 4°C.[5] Based on our data, even though the compound **16** and **17** was turned over quickly within the photo-activation period (3 min, **Figure 3A**), there were still plenty of **16** and **17** (>50%) in the reaction to ensure a good labeling of the sEH by the EET-PAL (**Figure 3A and S2**). In addition, the hydrolyzed products, 14,15-DHET and 14,15-DHET-PAL, of 14,15-EET and 14,15-EET-PAL respectively have poor affinity (K_i > 1 μM) toward sEH (**Figure S12**). Therefore, the labeling of the sEH is less likely to be due to its hydrolyzed product, corresponding 1,2-diol. The remaining epoxide hydrolase activity was also checked after the photolabeling experiment and the results showed that only 35% of the hydrolase activity was blocked. Therefore, a second round of photolabeling with the addition of corresponding EET-PAL was carried out. The result revealed that almost 50% of the sEH activity was blocked. (**Figure S6**) A further photolabeling cycle was not proceeded because this might lead to excessive photo-autoxidation of either the protein or the mimic and lead to degradation of the final photolabeled samples. The mass spectrometry analyses of the sEH photolabeled by different EET-PAL mimics showed that around 50% of the sEH was photolabeled by one molecule of EET-PAL (**16** and **17**) in all of these samples. (**Figure 3B** and **Figure S7**) Following the digestion of these samples by trypsin, the digested peptides were analyzed and sequenced by LC/MS-MS. Based on the MASCOT analyses, three peptides that were photolabeled by 11,12-EET-PAL **17** and two peptides were

photolabeled by 14,15-EET-PAL **16** were identified. (**Figure 3D**) (Table 1, ion score ≥ 18, $p<0.05$)

Interestingly, similar residues of the two identical peptides were labeled by both 11,12-EET-PAL **17** and 14,15-EET-PAL **16**. (**Table 1)** These two labeled peptides are located in the C-terminus domain of sEH but on different sides of the binding pocket (**Figure S3C**), indicating that there may be more than one binding orientation for the EET and EET mimics. To date, a crystal structure of covalent intermediate with any of the sEH substrates has not yet been reported. The binding orientation of EET in sEH remains unknown and the apparently EETs could bind to sEH in either orientation. Based on the crystal structures of sEH with a series of inhibitors with a carboxylate group that mimics that of the EETs, it was hypothesized that the disfavored interaction between the specific side chain of the binding pocket and the carboxylate of the ligand would dictate their binding orientation into the active site of the sEH. [22] Therefore, both 14,15-EET-PAL **16** and 11,12-EET-PAL **17** carrying the carboxylate biostere, acyl sulfonamide, should label the residue(s) on the same side of the binding pocket as the corresponding EET does. However, both 11,12-EET-PAL **17** and 14,15-EET-PAL **16** label the residues on both sides of the sEH binding pocket, indicating that for EET and probably other epoxy-lcPUFA, the carboxylate is not likely playing a major role in dictating the binding orientation of the substrates into the sEH catalytic cavity. These results imply that the other factors are more likely to play an important role in determining the binding orientation of the substrates, like the stereochemistry of the epoxide.

Computational Modeling of EETs in Human sEH Indicates that the Stereochemistry of Epoxide Dictates the Binding Orientation of the Substrate in Human sEH

In order to understand the structural determinants directing the binding of the endogenous substrates (the EETs) to sEH, computational approaches were used to model the binding of EETs to sEH. Because the mimics **16** and **17** were synthesized as racemic mixtures, and because sEH is known to be enantioselective (**Figure S8**), [65] we hypothesized that the two identified peptides from MASCOT analyses may be labeled by the two different enantiomers of the mimics, and that the configuration at the epoxide determines the binding orientation within the active site of sEH, in a similar fashion reported previously for soybean EH. [66] To test this hypothesis, both enantiomers (*R,S* and *S,R*) of each EET (six molecules total) were docked into a *holo*-crystal structure (PDB code:4JNC) with the bound inhibitor removed. However, out of thousands of docked poses, only a few (<10%) positioned the epoxide in an orientation that is ready for catalysis (**Table S3**). The urea inhibitors are tight binding inhibitors with nano or picomolar binding affinity that form a network of interactions around the catalytic site, thus pulling the surrounding residues closely around the inhibitor. This prevents the epoxide substrates from getting enough space to enter and to correctly fit into the active site of sEH. Our results align very well with the recent study conducted by Kotev *et al.*[67] Their results indicated that sEH has a very flexible active site which can accommodate inhibitors with different sizes and shapes. However, once sEH binds to its ligand, the enzyme would tailor its active site to better recognize the bound ligand through induced fit mechanism. Therefore, the ligand bound structure is not amendable for docking of other small molecules which have a very different structural

features than the bound ligand. Here, we hypothesize that the unbound structure of sEH in the solution is more flexible than the inhibitor bound structure.

To address this limitation, molecular dynamics simulations were used instead of simply docking the substrate into a rigid structure. First, simulations were carried out with a set of 15 sEH inhibitors bound to sEH. These selected inhibitors are structurally very different with a diverse potency on sEH (**Table S2**). All of these simulations were remarkably stable, which is evidence in RMSD time series plots (**Figure S17A,C**). As a specific example, the inhibitor conformation of the UC2389 simulation maintained a conformation essentially identical to the crystal structure (RMSD=0.66Å for the energy minimized, average structure) and matched the orientation determined by the photoaffinity labeling experiments (**Figure 4A**). Subsequent MMGBSA binding free energy analysis on the trajectories produced a good correlation (R^2=0.81) with the experiment values (**Figure S9**). In addition, for the two structurally different inhibitors (UC2389 and *t*-AUCB), which were crystalized with sEH, simulations were performed with the binding orientations as found in the crystallography (PDB code: 4OCZ and 3WKE respectively) and corresponding opposite orientations. The MMGBSA analysis correctly predicted the orientation in the crystal structures to have a lower (more favorable) energy. These results validated our simulation method.

We then performed simulations of all enantiomers of the EETs bound in two opposite orientations (three EETs with two enantiomers each in two opposite orientations yields twelve total simulations) in the same fashion as for the inhibitors.. The EET simulations were not nearly as stable as the inhibitor simulations (**Figure S17B**), and in five of the twelve orientations, the EETs completely moved out of the active site during the 500 ns simulation. The different binding behavior observed does not appear to be the result of a change in the protein structure or dynamics since the overall RMSD of the protein-ligand complex is only slightly larger for the EET simulations. Additionally, the residue-averaged atomic fluctuations are very similar for the protein with inhibitor bound or (**Figure S18 and S19,top**) or with EET bound (**Figure S19,bottom**). An exception was found in residues 498-506 which locate near the active site. These residues show larger fluctuations when an EET molecule exits the active site.

We performed MMGBSA analyses on the seven simulations in which the EET molecule remained bound and found only moderate binding affinities (−37 to −41 kcal/mol) as compared to the inhibitors that we evaluated above. This range of binding affinities (about 4 kcal/mol) is rather narrow in terms of MMGBSA results and did not provide any meaningful conclusion about the orientation preference. Based on the difference in stability between the inhibitor and EET simulations, it seems likely that the sEH protein in the crystal structures tunes its binding pocket to bind to transition state mimics. These tight binding inhibitors were designed to mimic the hypothetical transition state of the EETs, actual substrates, which usually have lower affinity. These results suggest that it is difficult to simulate the binding of non-transition state mimics or substrate into the crystal structures bound with the tight binding inhibitors because these structures are optimized for the binding of those high affinity inhibitors and the active site has been closed tightly around the bound inhibitors.

Interestingly, the sEH protein relaxed slightly during the simulation with the EET bound as compared to the inhibitor bound structures. Thus, the docking of the different EET regio- and stereo-isomers was attempted again using the enzyme conformation which was relaxed and minimized in the presence of a bound EET. The two simulated structures, corresponding to the 11*S*,12*R*-EET bound in both orientations, were used as protein models for docking. These simulated models were taken from the equilibrated and minimized structures in the molecular dynamics simulations. Docking of EETs with the relaxed structures greatly improved the number of docking poses in the ideal active site region (**Table S3**) for which the epoxides were well-positioned for nucleophilic attack by Asp335. Additionally, for these docking poses which were ready to be hydrolyzed by Asp335, there is a clear preference for all the *R,S* epoxides to bind in the same orientation, whereas the *S,R* epoxides bind in the opposite orientation (**Table S3 and Figure 4B and 4C**). These simulations suggest that the binding orientation of the substrates is likely dictated by the stereochemistry of the epoxide and could explain the results on how racemic mimics of EETs are able to label the residues on both sides of the binding pocket of sEH instead of one specific sides of the binding pocket (**Figure 4D**).

Conclusion

In this report, the photolabel mimics of the inhibitor of sEH and EETs were designed and synthesized. Our results from the photolabeling experiments suggest that the inhibitors are likely to bind the sEH in single orientation while each of the enantiomer of the racemic substrate binds to sEH in single orientation but in the opposite direction. The computational modeling indicates that the stereochemistry of the epoxide dictates the binding orientation of the substrate into the enzyme, whereas the specific interactions of the carboxylate in the EET are of lesser importance. The computational simulation also suggests that the C-terminus binding pocket of sEH could undergo a “breathing motion” in order to bind tightly to the potent transition state analogues (inhibitors) or to direct the loosely bound substrates in the position that is ready for the catalysis. The simulation procedure and methodology developed here would allow the screening and the identification of other endogenous or xenobiotic that could be hydrolyzed by sEH. These could lead us to further explore the other role played by sEH in human physiology. In fact, the photolabel mimics of EET could also be used to identify the unknown EET specific binding proteins/enzymes from tissue/cell lysates. These tools will also help us to better understand the biological effect of EET in human physiology.

Supplementary Material

Refer to Web version on PubMed Central for supplementary material.

Acknowledgements

This work is partially supported by the NIEHS grant R01 ES002710; NIEHS Superfund Research Program Grant P42 ES004699 and NIH CounterAct U54 NS079202. K.S.S.L. is partially supported by the NIH Pathway to Independence Award from NIH/NIEHS (K99 ES024806). This work also used computational resources from both the Triton Shared Computing Cluster at UCSD and the Extreme Science and Engineering Discovery Environment (XSEDE), which is supported by National Science Foundation grant no. ACI-1053575. M.K.G. acknowledges funding from National Institute of General Medical Sciences (GM61300). M.K.G. has an equity interest in and is a

cofounder and scientific advisor of VeraChem LLC. The author would also like to thank Prof. Frances Ann Walker at University of Arizona for providing the bacterial P450 BM3 (F87V) plasmid and Prof. Aldrin Gomes for help in analyzing the peptide sequencing data.

Abbreviation

TFA	trifluoroacetic acid
PAL	photoaffinity label
EET	epoxy-eicosatrienoic acid
sEH	soluble epoxide hydrolase
lcPUFA	long-chain polyunsaturated fatty acid
LC/MS-MS	Liquid Chromatography with tandem mass spectrometry

Reference

[1]. Morisseau, C.; Hammock, BD. Impact of Soluble Epoxide Hydrolase and Epoxyeicosanoids on Human Health. In: Insel, PA., editor. Annu. Rev. Pharmacol. Toxicol. Vol. 53. 2013. p. 37-58.2013

[2]. Fischer R, Spallek B, Qadri F, Konkel A, Marko L, Luft FC, Zeldin DC, Schirdewan A, Muller DN, Schunck WH. CYP2J2 overexpression prevents remodeling and atrial fibrillation in chronic beta-adrenergic hypertrophy. Eur. Heart J. 2011; 32:473–473.

[3]. Hye Khan MA, Fish B, Wahl G, Sharma A, Falck JR, Paudyal MP, Moulder JE, Imig JD, Cohen EP. Epoxyeicosatrienoic acid analogue mitigates kidney injury in a rat model of radiation nephropathy. Clinical science (London, England : 1979). 2016; 130:587–599.

[4]. Morin C, Fortin S, Rousseau E. 19,20-EpDPE, a bioactive CYP450 metabolite of DHA monoacyglyceride, decreases Ca2+ sensitivity in human pulmonary arteries. Am. J. Physiol. Heart Circ. Physiol. 2011; 301:H1311–H1318. [PubMed: 21821782]

[5]. Morisseau C, Inceoglu B, Schmelzer K, Tsai H-J, Jinks SL, Hegedus CM, Hammock BD. Naturally occurring monoepoxides of eicosapentaenoic acid and docosahexaenoic acid are bioactive antihyperalgesic lipids. J. Lipid Res. 2010; 51:3481–3490. [PubMed: 20664072]

[6]. Ulu A, Harris TR, Morisseau C, Miyabe C, Inoue H, Schuster G, Dong H, Iosif A-M, Liu J-Y, Weiss RH, Chiamvimonvat N, Imig JD, Hammock BD. Anti-inflammatory Effects of omega-3 Polyunsaturated Fatty Acids and Soluble Epoxide Hydrolase Inhibitors in Angiotensin-II-Dependent Hypertension. J. Cardiovasc. Pharmacol. 2013; 62:285–297. [PubMed: 23676336]

[7]. Ulu A, Lee KSS, Miyabe C, Yang J, Hammock BG, Dong H, Hammock BD. An Omega-3 Epoxide of Docosahexaenoic Acid Lowers Blood Pressure in Angiotensin-II-Dependent Hypertension. J. Cardiovasc. Pharmacol. 2014; 64:87–99. [PubMed: 24691274]

[8]. Zhang G, Panigrahy D, Mahakian LM, Yang J, Liu J-Y, Lee KSS, Wettersten HI, Ulu A, Hu X, Tam S, Hwang SH, Ingham ES, Kieran MW, Weiss RH, Ferrara KW, Hammock BD. Epoxy metabolites of docosahexaenoic acid (DHA) inhibit angiogenesis, tumor growth, and metastasis. Proc. Natl. Acad. Sci. U.S.A. 2013; 110:6530–6535. [PubMed: 23553837]

[9]. Zhou Y, Sun G-Y, Liu T, Duan J-X, Zhou H-F, Lee KS, Hammock BD, Fang X, Jiang J-X, Guan C-X. Soluble epoxide hydrolase inhibitor 1-trifluoromethoxyphenyl-3-(1-propionylpiperidin-4-yl) urea attenuates bleomycin-induced pulmonary fibrosis in mice. Cell Tissue Res. 2016; 363:399–409. [PubMed: 26310139]

[10]. Podolin PL, Bolognese BJ, Foley JF, Long E, Peck B, Umbrecht S, Zhang XJ, B. Schwartz P.Zhu, Xie WS, Quinn C, Qi HW, Sweitzer S, Chen S, Galop M, Ding Y, Belyanskaya SL, Israel DI, Morgan BA, Behm DJ, Marino JP, Kurali E, Barnette MS, Mayer RJ, Booth-Genthe CL, Callahan JF. In vitro and in vivo characterization of a novel soluble epoxide hydrolase inhibitor. Prostaglandins Other Lipid Mediat. 2013; 104:25–31. [PubMed: 23434473]

[11]. Wang L, Yang J, Guo L, Uyeminami D, Dong H, Hammock BD, Pinkerton KE. Use of a Soluble Epoxide Hydrolase Inhibitor in Smoke-Induced Chronic Obstructive Pulmonary Disease. Am. J. Respir. Cell Mol. Biol. 2012; 46:614–622. [PubMed: 22180869]

[12]. Sirish P, Li N, Timofeyev V, Zhang X-D, Wang L, Yang J, Lee KSS, Bettaieb A, Ma SM, Lee JH, Su D, Lau VC, Myers RE, Lieu DK, Lopez JE, Young JN, Yamoah EN, Haj F, Ripplinger CM, Hammock BD, Chiamvimonvat N. Molecular Mechanisms and New Treatment Paradigm for Atrial Fibrillation. Circ. Arrhythm. Electrophysiol. 2016; 9

[13]. Lee KSS, Liu J-Y, Wagner KM, Pakhomova S, Dong H, Morisseau C, Fu SH, Yang J, Wang P, Ulu A, Mate CA, Nguyen LV, Hwang SH, Edin ML, Mara AA, Wulff H, Newcomer ME, Zeldin DC, Hammock BD. Optimized Inhibitors of Soluble Epoxide Hydrolase Improve in Vitro Target Residence Time and in Vivo Efficacy. J. Med. Chem. 2014; 57:7016–7030. [PubMed: 25079952]

[14]. Inceoglu B, Wagner KM, Yang J, Bettaieb A, Schebb NH, Hwang SH, Morisseau C, Haj FG, Hammock BD. Acute augmentation of epoxygenated fatty acid levels rapidly reduces pain-related behavior in a rat model of type I diabetes. Proc. Natl. Acad. Sci. U.S.A. 2012; 109:11390–11395. [PubMed: 22733772]

[15]. Shen HC. Soluble epoxide hydrolase inhibitors: a patent review. Expert Opin. Ther. Pat. 2010; 20:941–956. [PubMed: 20429668]

[16]. Amano Y, Tanabe E, Yamaguchi T. Identification of N-ethylmethylamine as a novel scaffold for inhibitors of soluble epoxide hydrolase by crystallographic fragment screening. Bioorg. Med. Chem. 2015; 23:2310–2317. [PubMed: 25862210]

[17]. Argiriadi MA, Morisseau C, Goodrow MH, Dowdy DL, Hammock BD, Christianson DW. Binding of alkylurea inhibitors to epoxide hydrolase implicates active site tyrosines in substrate activation. J. Biol. Chem. 2000; 275:15265–15270. [PubMed: 10747889]

[18]. Argiriadi MA, Morisseau C, Hammock BD, Christianson DW. Detoxification of environmental mutagens and carcinogens: Structure, mechanism, and evolution of liver epoxide hydrolase. Proc. Natl. Acad. Sci. U.S.A. 1999; 96:10637–10642. [PubMed: 10485878]

[19]. Morisseau C, Pakhomova S, Hwang SH, Newcomer ME, Hammock BD. Inhibition of soluble epoxide hydrolase by fulvestrant and sulfoxides. Bioorg. Med. Chem. Lett. 2013; 23:3818–3821. [PubMed: 23684894]

[20]. Pecic S, Pakhomova S, Newcomer ME, Morisseau C, Hammock BD, Zhu Z, Deng S. 4HAI: Crystal structure of human soluble epoxide hydrolase complexed with N-cycloheptyl-1-(mesitylsulfonyl)piperidine-4-carboxamide. Worldwide Protein Data Bank. 2012

[21]. Xue Y, Olsson T, Johansson CA, Oster L, Beisel H-G, Rohman M, Karis D, Backstrom S. Fragment Screening of Soluble Epoxide Hydrolase for Lead GenerationStructure-Based Hit Evaluation and Chemistry Exploration. Chemmedchem. 2016; 11:497–508. [PubMed: 26845235]

[22]. Gomez GA, Morisseau C, Hammock BD, Christianson DW. Human soluble epoxide hydrolase: Structural basis of inhibition by 4-(3-cyclohexylureido)-carboxylic acids. Prot. Sci. 2006; 15:58–64.

[23]. Bikker JA, Trumpp-Kallmeyer S, Humblet C. G-protein coupled receptors: Models, mutagenesis, and drug design. J. Med. Chem. 1998; 41:2911–2927. [PubMed: 9685229]

[24]. Bradley SJ, Tobin AB. Insel PA. Design of Next-Generation G Protein-Coupled Receptor Drugs: Linking Novel Pharmacology and In Vivo Animal Models. Annu. Rev. Pharmacol. Toxicol. 562016:535–559.

[25]. Ford KA, Ryslik G, Sodhi J, Halladay J, Diaz D, Dambach D, Masuda M. Computational predictions of the site of metabolism of cytochrome P450 2D6 substrates: comparative analysis, molecular docking, bioactivation and toxicological implications. Drug Metab. Rev. 2015; 47:291–319. [PubMed: 26024250]

[26]. Goldsmith EJ, Akella R, Min XS, Zhou TJ, Humphreys JM. Substrate and docking interactions in serine/threonine protein kinases. Chem. Rev. 2007; 107:5065–5081. [PubMed: 17949044]

[27]. Mo SL, Liu WF, Li CG, Zhou ZW, Luo HB, Chew H, Liang J, Zhou SF. Pharmacophore, QSAR, and Binding Mode Studies of Substrates of Human Cytochrome P450 2D6 (CYP2D6) Using Molecular Docking and Virtual Mutations and an Application to Chinese Herbal Medicine Screening. Curr. Pharm. Biotechnol. 2012; 13:1640–1704. [PubMed: 22039821]

[28]. Moser D, Achenbach J, Klingler FM, Ia BE, Hahn S, Proschak E. Evaluation of structure-derived pharmacophore of soluble epoxide hydrolase inhibitors by virtual screening. Bioorg. Med. Chem. Lett. 2012; 22:6762–6765. [PubMed: 23017883]

[29]. Oster L, Tapani S, Xue YF, Kack H. Successful generation of structural information for fragment-based drug discovery. Drug Discov. Today. 2015; 20:1104–1111. [PubMed: 25931264]

[30]. Roy J, Cyert MS. Cracking the Phosphatase Code: Docking Interactions Determine Substrate Specificity. Sci. Signal. 2009; 2

[31]. Reddy KK, Vidya Rajan VK, Gupta A, Aparoy P, Reddanna P. Exploration of binding site pattern in arachidonic acid metabolizing enzymes, Cyclooxygenases and Lipoxygenases. BMC Res Notes. 2015; 8

[32]. Chen H, Zhang Y, Li L, Han JG. Probing Ligand-Binding Modes and Binding Mechanisms of Benzoxazole-Based Amide Inhibitors with Soluble Epoxide Hydrolase by Molecular Docking and Molecular Dynamics Simulation. J. Phys. Chem. B. 2012; 116:10219–10233. [PubMed: 22857012]

[33]. Xing L, McDonald JJ, Kolodziej SA, Kurumbail RG, Williams JM, Warren CJ, O'Neal JM, Skepner JE, Roberds SL. Discovery of Potent Inhibitors of Soluble Epoxide Hydrolase by Combinatorial Library Design and Structure-Based Virtual Screening. J. Med. Chem. 2011; 54:1211–1222. [PubMed: 21302953]

[34]. Waltenberger B, Garscha U, Temml V, Liers J, Werz O, Schuster D, Stuppner H. Discovery of Potent Soluble Epoxide Hydrolase (sEH) Inhibitors by Pharmacophore-Based Virtual Screening. J. Chem. Inf. Model. 2016; 56:747–762. [PubMed: 26882208]

[35]. Lonsdale R, Hoyle S, Grey DT, Ridder L, Mulholland AJ. Determinants of Reactivity and Selectivity in Soluble Epoxide Hydrolase from Quantum Mechanics/Molecular Mechanics Modeling. Biochemistry. 2012; 51:1774–1786. [PubMed: 22280021]

[36]. Hopmann KH, Himo F. Insights into the reaction mechanism of soluble epoxide hydrolase from theoretical active site mutants. J. Phys. Chem. B. 2006; 110:21299–21310. [PubMed: 17048959]

[37]. Hopmann KH, Himo F. Theoretical study of the full reaction mechanism of human soluble epoxide hydrolase. Chem. Eur. J. 2006; 12:6898–6909. [PubMed: 16856182]

[38]. Lindberg D, Revenga MD, Widersten M. Temperature and pH Dependence of Enzyme-Catalyzed Hydrolysis of trans-Methylstyrene Oxide. A Unifying Kinetic Model for Observed Hysteresis, Cooperativity, and Regioselectivity. Biochemistry. 2010; 49:2297–2304. [PubMed: 20146441]

[39]. Dorman G, Prestwich GD. Using photolabile ligands in drug discovery and development. Trends Biotechnol. 2000; 18:64–77. [PubMed: 10652511]

[40]. Ranade AR, Higgins L, Markowski TW, Glaser N, Kashin D, Bai R, Hong KH, Hamel E, Hoefle G, Georg GI. Characterizing the Epothilone Binding Site on beta-Tubulin by Photoaffinity Labeling: Identification of beta-Tubulin Peptides TARGSQQY and TSRGSQQY as Targets of an Epothilone Photoprobe for Polymerized Tubulin. J. Med. Chem. 2016; 59:3499–3514. [PubMed: 26986898]

[41]. Safa AR, Glover CJ, Meyers MB, Biedler JL, Felsted RL. Vinblastine photoaffinity-labeling of a high molecular-weight surface-membrane glycoprotein specific for multidrug-resistant cells. J. Biol. Chem. 1986; 261:6137–6140. [PubMed: 3700389]

[42]. Vanderbend RL, Brunner J, Jalink K, Vancorven EJ, Moolenaar WH, Vanblitterswijk WJ. Identification of a putative membrane-receptor for the bioactive phospholipid, lysophosphatidic acid. Embo J. 1992; 11:2495–2501. [PubMed: 1321033]

[43]. Morisseau C, Beetham JK, Pinot F, Debernard S, Newman JW, Hammock BD. Cress and potato soluble epoxide hydrolases: Purification, biochemical characterization, and comparison to mammalian enzymes. Arch. Biochem. Biophys. 2000; 378:321–332. [PubMed: 10860549]

[44]. Schwaneberg U, Sprauer A, Schmidt-Dannert C, Schmid RD. P450 monooxygenase in biotechnology - I. Single-step, large-scale purification method for cytochrome P450BM-3 by anion-exchange chromatography. J. Chromatogr. A. 1999; 848:149–159. [PubMed: 10427755]

[45]. Guengerich FP, Martin MV, Sohl CD, Cheng Q. Measurement of cytochrome P450 and NADPH-cytochrome P450 reductase. Nat. Protoc. 2009; 4:1245–1251. [PubMed: 19661994]

[46]. Borhan B, Mebrahtu T, Nazarian S, Kurth MJ, Hammock BD. Improved radiolabeled substrates for soluble epoxide hydrolase. Anal. Biochem. 1995; 231:188–200. [PubMed: 8678300]

[47]. Allen WJ, Balius TE, Mukherjee S, Brozell SR, Moustakas DT, Lang PT, Case DA, Kuntz ID, Rizzo RC. DOCK 6: Impact of new features and current docking performance. J. Comput. Chem. 2015; 36:1132–1156. [PubMed: 25914306]

[48]. Reema KT, McAtee JJ, Belyanskaya S, Brandt M, Brown GD, Costell MH, Ding Y, Dodson JW, Eisennagel SH, Fries RE, Gross JW, Harpel MR, Holt DA, Israel DI, Jolivette LJ, Krosky D, Li H, Lu QN, Mandichak T, Roethke T, Schnackenberg CG, Schwartz B, Shewchuk LM, Xie WS, Behm DJ, Douglas SA, Shaw AL, Marino JP. Discovery of 1-(1,3,5-triazin-2-yl)piperidine-4-carboxamides as inhibitors of soluble epoxide hydrolase. Bioorg. Med. Chem. Lett. 2013; 23:3584–3588. [PubMed: 23664879]

[49]. Anandakrishnan R, Aguilar B, Onufriev AV. H++3.0: automating pK prediction and the preparation of biomolecular structures for atomistic molecular modeling and simulations. Nucleic Acids Res. 2012; 40:W537–W541. [PubMed: 22570416]

[50]. Pettersen EF, Goddard TD, Huang CC, Couch GS, Greenblatt DM, Meng EC, Ferrin TE. UCSF chimera - A visualization system for exploratory research and analysis. J. Comput. Chem. 2004; 25:1605–1612. [PubMed: 15264254]

[51]. Desjarlais RL, Sheridan RP, Seibel GL, Dixon JS, Kuntz ID, Venkataraghavan R. Using shape complementarity as an initial screen in designing ligands for a receptor-binding site of known 3-dimensional structure. J. Med. Chem. 1988; 31:722–729. [PubMed: 3127588]

[52]. Meng EC, Shoichet BK, Kuntz ID. AUTOMATED DOCKING WITH GRID-BASED ENERGY EVALUATION. J. Comput. Chem. 1992; 13:505–524.

[53]. Case, DA.; Betz, RM.; Botello-Smith, W.; Cerutti, DS.; Cheatham, I.; T.A. Darden, TE,.; Duke, RE.; Gohlke, H.; Goetz, AW.; Gusarov, S.; Homeyer, N.; Janowski, P.; Kaus, J.; Kolossváry, I.; Kovalenko, A.; Lee, TS.; LeGrand, S.; Luchko, T.; Luo, R.; Madej, B.; Merz, KM.; Paesani, F.; Roe, DR.; Roitberg, A.; Sagui, C.; Salomen-Ferrer, R.; Seabra, G.; Simmerling, CL.; Smith, W.; Swails, J.; Walker, RC.; Wang, J.; Wolf, RM.; Wu, X.; Kollman, PA.; 14, Amber. University of California at San Francisco. 2014.

[54]. Jakalian A, Bush BL, Jack DB, Bayly CI. Fast, efficient generation of high-quality atomic charges. AM1-BCC model: I. Method. J. Comput. Chem. 2000; 21:132–146.

[55]. Jakalian A, Jack DB, Bayly CI. Fast, efficient generation of high-quality atomic charges. AM1-BCC model: II. Parameterization and validation. J. Comput. Chem. 2002; 23:1623–1641. [PubMed: 12395429]

[56]. Wang J, Wolf RM, Caldwell JW, Kollman PA, Case DA. Development and testing of a general amber force field. J. Comput. Chem. 2004; 25:1157–1174. [PubMed: 15116359]

[57]. Jorgensen WL, Chandrasekhar J, Madura JD, Impey RW, Klein ML. Comparison of simple potential functions for simulating liquid water. J. Chem. Phys. 1983; 79 926.

[58]. Joung IS, Cheatham TE. Determination of Alkali and Halide Monovalent Ion Parameters for Use in Explicitly Solvated Biomolecular Simulations. J. Phys. Chem. B. 2008; 112:9020–9041. [PubMed: 18593145]

[59]. Henriksen NM, Fenley AT, Gilson MK. Computational Calorimetry: High-Precision Calculation of Host-Guest Binding Thermodynamics. J. Chem. Theory Comput. 2015; 11:4377–4394. [PubMed: 26523125]

[60]. Hopkins CW, Le Grand S, Walker RC, Roitberg AE. Long-Time-Step Molecular Dynamics through Hydrogen Mass Repartitioning. Journal of Chemical Theory Comput. 2015; 11:1864–1874.

[61]. Miller BR, McGee TD, Swails JM, Homeyer N, Gohlke H, Roitberg AE. MMPBSA.py: An Efficient Program for End-State Free Energy Calculations. J. Chem. Theory and Computation. 2012; 8:3314–3321.

[62]. Tate JJ, Persinger J, Bartholomew B. Survey of four different photoreactive moieties for DNA photoaffinity labeling of yeast RNA polymerase III transcription complexes. Nucleic Acids Res. 1998; 26:1421–1426. [PubMed: 9490787]

[63]. Falck JR, Krishna UM, Reddy YK, Kumar PS, Reddy KM, Hittner SB, Deeter C, Sharma KK, Gauthier KM, Campbell WB. Comparison of vasodilatory properties of 14,15-EET analogs: structural requirements for dilation. Am. J. Physiol. Heart Circ. Physiol. 2003; 284:H337–H349. [PubMed: 12388250]

[64]. Lassalas P, Gay B, Lasfargeas C, James MJ, Van T, Vijayendran KG, Brunden KR, Kozlowski MC, Thomas CJ, Smith AB III, Huryn DM, Ballatore C. Structure Property Relationships of Carboxylic Acid Isosteres. J. Med. Chem. 2016; 59:3183–3203. [PubMed: 26967507]

[65]. Zeldin DC, Wei SZ, Falck JR, Hammock BD, Snapper JR, Capdevila JH. Metabolism of epoxyeicosatrienoic acids by cytosolic epoxide hydrolase - substrate structural determinants of asymmetric catalysis. Arch.Biochem. Biophys. 1995; 316:443–451. [PubMed: 7840649]

[66]. Blee E, Schuber F. Regioselectivity and enantioselectivity of soybean fatty-acid epoxide hydrolase. J. Biol. Chem. 1992; 267:11881–11887. [PubMed: 1601858]

[67]. Kotev M, Soliva R, Orozco M. Challenges of docking in large, flexible and promiscuous binding sites. Bioorg. Med. Chem. 2016; 24:4961–4969. [PubMed: 27545443]

Highlights

- sEH inhibitor and EET photolabel mimics have been synthesized.
- These photolabel mimics can be used to identify the binding site of EET in sEH.
- The carboxylate of EET does not play an important role in its binding to sEH.
- The binding orientation of EET is dictated by the stereochemistry of its epoxide.
- A new computational model can predict how inhibitors and epoxides bind to sEH.

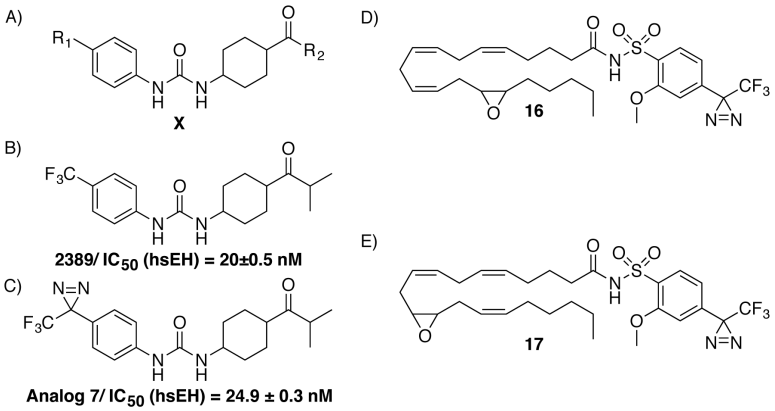

Figure 1.

A) The general scaffold of one of the leading series of sEH inhibitors; **B)** Structure of UC2389; **C)** The photoaffinity analog of UC2389 (**7**); **D)** The 14,15-EET-PAL (**16**) and; **E)** The 11,12-EET-PAL (**17**)

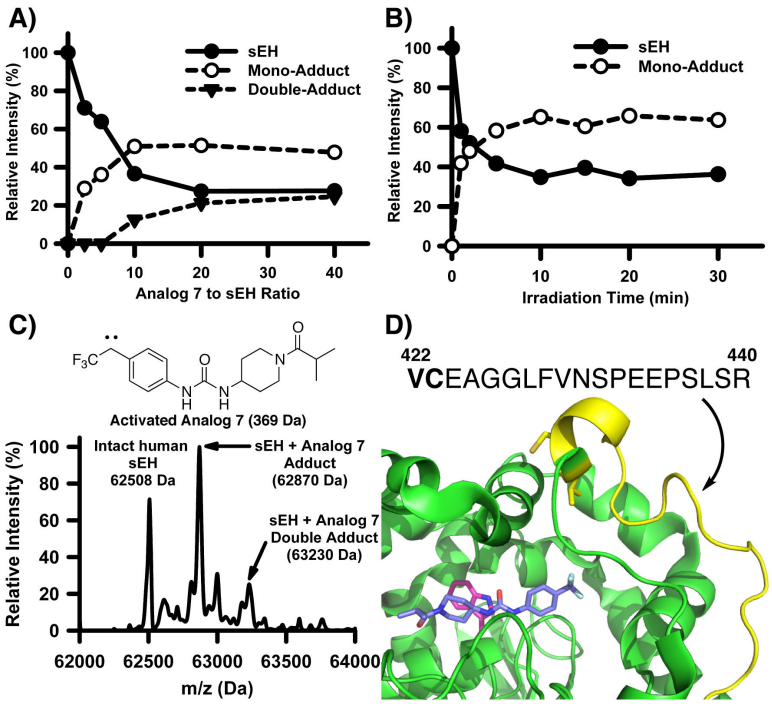

Figure 2.

A) The optimum ratio of analog **7** to sEH is 10 to 1 based on intact mass spectrometric analysis; **B)** Majority of human sEH was labeled after 5 min of irradiation at 365 nm; **C)** Mass spectrometric analysis of intact sEH photolabeled by analog **7** and; **D)** MASCOT analyses (minimum ion score ≥18) identified residues Val and/or Cys within the peptide 422-440 (shown as yellow; ion score 70) was labeled by analog **7**. The crystal structure (PDB code: 4OCZ) shown that the identified peptide was located on the right side of the binding pocket. The inhibitor UC2389 is shown as blue stick to indicate the location of the C-terminus active site of human sEH.

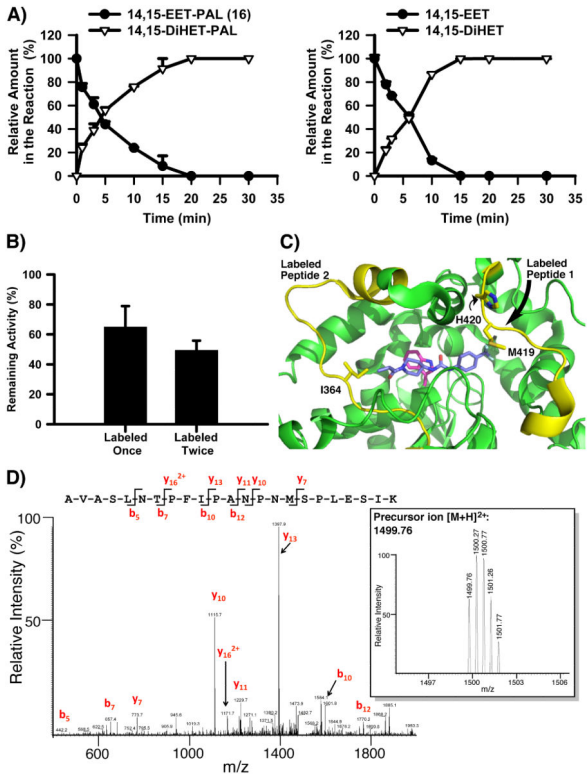

Figure 3.

A) The rate of hydrolysis of 14,15-EET-PAL **16** and 14,15-EET by human sEH is similar; **3B)** LC/MS analysis of the human sEH photolabeled by 11,12-EET-PAL **17**; **3C)** The identified peptides at C-terminus domain photolabeled by EET-PAL **16** and **17** based on MASCOT analyses of human sEH are highlighted in yellow with the residues labeled by 14,15-EET-PAL **17** shown as stick; **3D)** The representative LC/MS-MS spectrum of one of the identified peptides (AVASLNTPFIPANPNMSPLESIK) photolabeled by 11,12-EET-PAL (587.25 Da) with the identified fragmented peak indicated and labeled. The identified fragmented peaks indicate that the 11,12-EET-PAL labels the residues between F, I and/or P. In addition, the corresponding precursor ion $[M+H]^{2+}$ spectrum was also shown. The exact mass of the precursor ion (m/z = 1499.76) matches the predicted adduct mass ion (m/z = 1499.13).

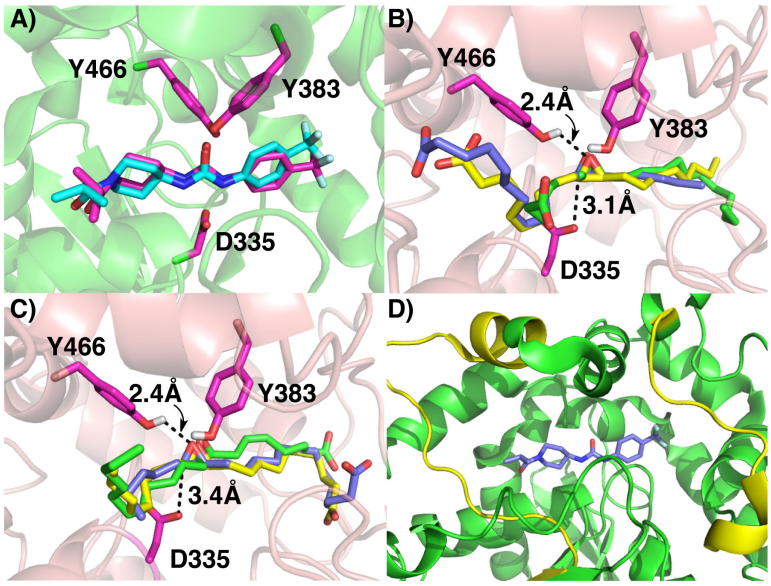

Figure 4.

A) The overlay between crystal structure (PDB code: 4OCZ) of human sEH with UC2389 (shown as cyan) and the model of human sEH bound with UC2389 (purple) with three catalytic residues: Y466, Y383 and D335 shown and labeled; **B)** The models of human sEH bound with 8*R*, 9*S*-EET (green), 11*R*, 12*S*-EET (yellow) and 14*R*,15*S*-EET (purple) with three catalytic residues: Y466, Y383 and D335 shown and labeled. The epoxides with same stereochemistry binds to human sEH in the same orientation; **C)** The models of human sEH bound with 8*S*, 9*R*-EET (green), 11*S*, 12*R*-EET (yellow) and 14*S*,15*R*-EET (purple) with three catalytic residues: Y466, Y383 and D335 shown and labeled. The epoxides with same stereochemistry binds to human sEH in the same orientation and; **D)** MASCOT analyses identified the two identical peptides (shown as yellow in the structure) that are labeled by both EET-PAL **16** and **17**. The crystal structure (PDB code: 4OCZ) indicated that these two photolabeled peptides (as shown as yellow in structure) are located at both side of the binding pocket at the C-terminal domain of human sEH. The inhibitor 2389 (shown as blue stick) indicated the location of the binding site in the crystal structure.

Table 1

The sequence of the labeled peptides that were identified by MASCOT search from the samples of human sEH photolabeled by EET-PAL analogs. Possible labeled residues are highlighted in BOLD.

11,12-EET-PAL **17**			
Labeled Peptide Index	Residue No.	Ion score	Labeled Peptides Sequence
sEH-**17** #1	411-421	20	ASDESVLS**MH**K
sEH-**17** #2	354-376	18	AVASLNT**PFI**PANPNMSPLESIK
sEH-**17** #3	44-52	20	GGPEGAT**TR**
14,15-EET-PAL **16**			
Labeled Peptide Index	Residue No.		Labeled Peptides Sequence
sEH-**16** #1	411-421	21	ASDESVLS**MH**K
sEH-**16** #2	354-376	26	AVASLNTPF**I**PANPNMSPLESIK

Table E1

Mass Spectrometry Parameters:

System:	**Water Ultima^{TM} ESI (−)**
Cone Voltage:	120V
Capillary Voltage:	1.6 kV
Desolution Temperature	260 °C
Source Temperature	100 °C
Scan time:	10 min
Scan range:	1500 to 2500 m/z

Table E2

Online Desalting Protocol (Solvent A: Water with 0.1% Formic Acid; Solvent B: Acetonitrile with 0.1% Formic Acid):

Step	Time (min)	%B
1	0 – 2	5
2	2 – 3.1	5 to 50 (linear)
3	3.1 – 4.5	50 to 85 (linear)
4	4.5 – 7.5	98
5	7.5 – 10	5

Table E3

LC Protocol (Solvent A: Water with 0.1% Acetic Acid; Solvent B: Acetonitrile with 0.1% Acetic Acid):

Step	Time (min)	%B
1	0 – 1.1	60
2	1.1-3.0	60 to 100 (linear)
3	3.0-3.4	100
4	3.4-3.5	100 to 60
5	3.5-4.5	60

Table E4

Optimized conditions for monitoring parent 14,15-EET, 14,15-DiHET, 14,15-EET-PAL 16, 14,15-DiHET-PAL by MRM on 4000 Q-TRAP triple quadrupole mass spectrometer

Compound	Transition (Q1-Q3)	Declustering Potential (V)	Entrance Potential (V)	Collision Energy (V)	Collision Cell Exit Potential (V)	LOD (nM)
14,15-EET	319.200-219.300	−65	−10	−25	−10	≤0.25
14,15-DiHET	337.200-207.100	−65	−10	−20	−4	≤0.25
14,15-EET-PAL (**16**)	596.126-568.200	−45	−10	−22	−15	≤0.49
14,15-DiHET-PAL	614.265-169.000	−40	−10	−28	−15	≤0.49
11,12-EET	319.303-167.200	−60	−10	−20	−7	≤0.49
11,12-DiHET	337.200-167.100	−65	−10	−26	−8	≤0.49
11,12-EET-PAL (**16**)	596.126-568.200	−55	−10	−22	−13	≤0.49
11,12-DiHET-PAL	614.265-169.00	−35	−10	−26	−7	≤0.49